International Journal of Biological Macromolecules 216 (2022) 676–685

Contents lists available at ScienceDirect

International Journal of Biological Macromolecules

journal homepage: www.elsevier.com/locate/ijbiomac

Effective biosorption of Cu(II) using hybrid biocomposite based on N-maleated chitosan/calcium alginate/titania: Equilibrium sorption, kinetic and thermodynamic studies

Hamza Shehzad [a,*], Zahoor H. Farooqi [a,*], Ejaz Ahmed [a], Ahsan Sharif [a], Muhammad Ajmal [b], Sana Razzaq [a], M. Uzair Naseer [a], M. Ahmad Nazir [a], Mehwish Batool [a], Tehreem Akram [a], Qamar un Nissa [a], Amarah Fatima [a], Laiba Akbar [a]

[a] School of Chemistry, University of the Punjab, Lahore 54590, Pakistan
[b] Department of Chemistry, Division of Science and Technology, University of Education, Lahore, Pakistan

ARTICLE INFO

Keywords:
N-maleated chitosan
Chemically modified calcium alginate
Titania encapsulation
Cu(II) biosorption

ABSTRACT

In this research work, a hybrid biocomposite based on N-maleated chitosan, amino-thiocarbamate functionalised calcium alginate and anhydrous Titania nanoparticles (NMC-MCA-TiO_2) was fabricated. The study involves the one pot facile synthesis of N-maleated chitosan and amino-thiocarbamate functionalised alginate under moderate conditions. Sorbent was conditioned in the form of hydrogel beads and characterized through FT-IR and SEM analysis. Newly grafted functional groups could act as potential chelating sites for enhanced Cu(II) sorption. Modified biopolymers were organo-functionalised which provided excellent support for immobilization of Titania nanoparticles (TiO_2) as inorganic filler. Kinetic data illustrated the manifestation of intrinsic chemisorption instead of simple bulk/film diffusion. Equilibrium sorption data fitted well with Freundlich adsorption model ($R^2 \approx 0.99$) which designated the heterogeneous nature of sorbent. Maximum sorption capacity of biosorbent was found 192 mg/g at 298 K and pH = 6.0. Standard Gibbs free energy change ΔG^o (−21.53, −21.97, and − 22.42 kJ/mol), standard enthalpy change ΔH^o (5.12 kJ/mol) and standard entropy change ΔS^o (0.09 kJ/mol K^{-1}) values suggested that the sorption process to be spontaneous and endothermic. The sorbent 3NMC-MCA-TiO_2 could be competitive candidate for economical and rapid adsorptive removal of Cu(II) from dilute contaminated liquids.

1. Introduction

Hypertoxic heavy metal remediation from waste water containing dilute concentration of contaminants is particularly challenging on account of their bioaccumulation and adverse effects on our biological ecosystem [1]. Therefore, environmental risk management associated with remediation of toxic metal from areas having limited water resources has been a hot topic in recent research. Copper is among the major heavy metal pollutants liberated extensively as industrial and agricultural wastes which induces serious health concerns to living organisms at concentrations exceeding 1.3 mg/L as per EPA (Environmental Protection Agency) recommendations [2,3]. In human body, the paramount importance of copper traces for normal homeostasis and haemoglobin functioning is well-known. However, copper poisoning may also lead to gastrointestinal illness, hypertension, emesis, Wilson's disease, insomnia, cancer, hepatic disorder and renal failure. Therefore, several physiochemical, chemical, electrochemical, and biological methods have recently been developed to sequestrate copper from dilute aqueous solutions [4]. The frequently practised conventional methods related to remediation of copper from polluted water include: chemical precipitation [5], floatation [6], coagulation [7], electro-deposition [8], ion-exchange methods [9], reverse osmosis [10], adsorption [11] and membrane filtration [12] etc. Adsorption is considered as a potential and most promising method for small-scale recovery of metal ions on account of its easy operation, appreciable efficiency, reusability of materials and low cost. In this context, several types of organic and inorganic adsorbent materials have been reported for effective copper removal. [13–22]. Biosorbents with biological origin have attracted more interest in recent studies because of their economic and environment friendly approach.

* Corresponding authors at: School of Chemistry, University of the Punjab, Lahore 54590, Pakistan.
E-mail addresses: hamzashehzad89@yahoo.com (H. Shehzad), zahoor.chem@pu.edu.pk (Z.H. Farooqi).

https://doi.org/10.1016/j.ijbiomac.2022.06.159
Received 18 April 2022; Received in revised form 27 May 2022; Accepted 25 June 2022
Available online 8 July 2022

Chitosan and alginate based polysaccharides have been found as promising biosorbents for the sorption of heavy metal ions from polluted water [23]. Chitosan is a linear polysaccharide having intrinsic chelating ability owing to the presence of amino and hydroxyl functionalities. It could be derived economically and in good yield from chitin after basic deacetylation. Moreover, physicochemical properties of chitosan could be improved through several interesting chemical modifications [9,24]. Sodium alginate (SA) is an natural biopolymer which is generally extracted from brown seaweed having linear molecular chains of β-D-mannuronate (M) and α-L-guluronate (G) with numerous hydroxyl (-OH) and carboxylic (-COOH) groups attached over it [25]. Ionotropic gelation of SA with divalent cations such as Ba^{2+} Ca^{2+}, Sr^{2+} and Fe^{3+} produce three-dimensional metal crosslinked gels [26]. Recent researches have reported this green biopolymer as nontoxic, biodegradable, biocompatible, abundant and environment-friendly thus proposing it as an effective candidate for convenient recovery of heavy metals from aqueous media [27]. However, less stability, poor water resistance and serious thermal degradation associated with it might lower its sorption capacity towards heavy metal ions owing to loose molecular network of gels. So, a simple and effective solution is to modify the chitosan and alginate network to produce chemically modified derivatives with suitable structures possessing high sorption capacity and mechanical strength [28]. Moreover, several novel surface modifications and compositions with inorganic fillers have been introduced into chitosan and alginate matrix to induce good mechanical strength [29–31].

In present work we fabricated a hybrid biocomposite based on N-maleated chitosan/calcium alginate/titania (NMC-MCA-TiO_2). The one pot facile synthesis of N-maleated chitosan and amino-thiocarbamated alginate under moderate conditions. These modifications provided an excellent encapsulation for Titania nanoparticles (TiO_2) as an inorganic filler. After this physio-chemical functionalization the sorbent was conditioned in the form of hydrogel beads. This modification introduced variety of functional sites such as: -CO-CH=CH-COOH, -OH, -NH_2, -O-CS-$NHNH_2$ over the sorbent surface to improve overall efficiency and sorption capacity of base biopolymers. The NMC-MCA-TiO_2 composite beads were employed successfully for sorption of Cu(II) ions and found highly efficient. Employed analytical techniques provided the evidence of successful chemical modification and Cu(II) sorption. The various sorption parameters such as pH, temperature, sorbent dosage, contact time and initial metal concentration were investigated and optimized for enhanced Cu(II) sorption. Kinetic and isothermal sorption studies were carried out in detail to understand the sorption phenomenon. The sorption mechanism of Cu(II) using NMC-MCA-TiO_2 composite beads was also proposed accordingly.

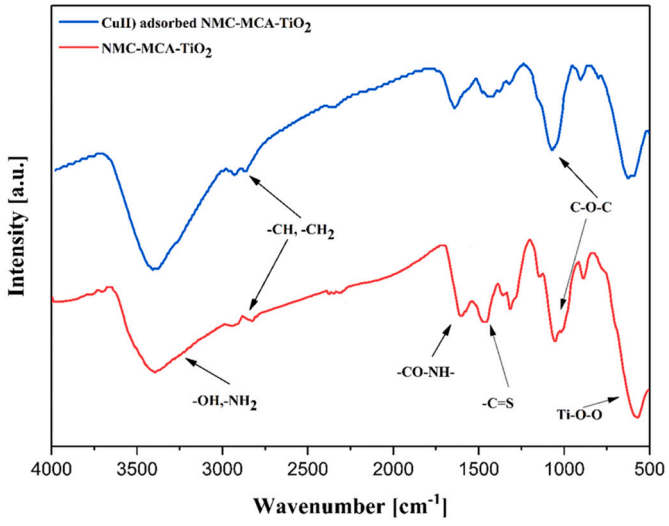

Fig. 1. Stacked FTIR spectra of newly developed sorbent (3NMC-MCA-TiO_2) and Cu(II) adsorbed 3NMC-MCA-TiO_2.

2. Experimental

2.1. Required chemicals

Chitosan (CS, mol. weight 8.55 × 10^5 kDa, highly pure, dynamic viscosity equals to 50–800 mPa.s, degree of deacetylation D.D. ≥ 80 %) and sodium alginate (SA, purity ≥99.5 %, guluronic acid ratio equals to 35.5 %) was supplied by Chem. Pure chemical company, pvt. Ltd. (Lahore, Pakistan). Dimethyl sulfoxide solvent, DMSO (99.5 %), Thiosemicarbazide (TSC, 99.9 %), Maleic anhydride (MA, 99.5 %), Epichlorohydrin (ECH, 99.8 %) and Formic acid (99.8 %), $CaCl_2$ (reagent grade) were Sigma-Aldrich products and were utilized without further treatment. Copper (1000 ppm) stock solution was prepared by dissolving appropriate amount of Copper (II) nitrate hexahydrate (99.99 %, Merck) in ultrapure water.

2.2. Instrumentation

FT-IR characterization of the sorbent (3NMC-MCA-TiO_2) and precursors were carried out using Nicolet, Magna-550 spectrometer equipped with a diamond crystal, at scanning range of 4000–500 cm^{-1}. Apparent texture and surface morphology was studied by FE-SEM (JEOL, JSM-7500F) scanning electron microscope which could achieve a resolution of 1.5 nm at 1 kV. Smooth and continuous rotational uniform sorption was performed in the form batch mode operation using Orbital shaker (Model: JISICO, Germany). Copper concentrations were estimated on ICP-OES (iCAP-7600, Thermo Fischer Scientific, UK) and some samples were also analysed on AAS (iCE-3000 series, Thermo Fischer Scientific, UK).

2.3. Synthesis of biocomposite (NMC-MCA-TiO_2)

Chitosan was organo-functionalized with maleic anhydride as per our previous reported work [32]. In first step, CS (4.0 g) and maleic anhydride (4.0 g) were taken in a round bottom flask containing DMSO (100.0 mL) and stirred for 1 h. Then, contents were refluxed at 90 °C for 8 h. The product (NMC) was obtained by quenching the reaction using acetone (200.0 mL). Solid product filtered, rinsed with acetone and vacuum dried. Secondly, SA (4.0 g) and TSC (2.0 g) were mixed in another round bottom flask containing deionized water (100.0 mL). Mixture was refluxed at 100 °C for 4 h with continuous stirring [33]. After reaction, the thick slurry of modified SA was equally distributed to four labeled beakers i.e., I, II, III, I*V*. Equal amounts of NMC i.e., 1.0 g was added to these beakers. Then, variable amounts of rutile (TiO_2) i.e., 0.050, 0.075, 0.100, 0.150 g were added to labeled beakers, respectively, to get different composition of TiO_2 in NMC-MCA (5.0–15.0 % by weight). The contents of beakers were thoroughly stirred for 1.5 h which lead to the homogeneous mixtures. After that, hydrogel beads were formed by ionotropic gelation using $CaCl_2$ saturated solution and obtained beads were designated as 1NMC-MCA-TiO_2, 2NMC-MCA-TiO_2/TSC-CA, 3NMC-MCA-TiO_2 and 4NMC-MCA-TiO_2, respectively.

2.4. Sorption and kinetic experiments methodology

A series of sorption experiments were conducted by preparing the standard aqueous solutions of Cu(II) by adding appropriate calculated amounts of copper salt in deionized water. The experiments were performed at optimized pH value 6.0 by shaking 180 mg of hydrogel beads with 25 mL of standard Cu(II) solution over wide concentration ranges (25–300 mg/L) for 3 h equilibrium time as observed in kinetic studies in incubate shaker at different temperatures (298, 303 and 308 K), at rotation speed of orbital shaker at 150 rpm to ensure better diffusion. Similar conditions were employed in kinetic experiments as well by

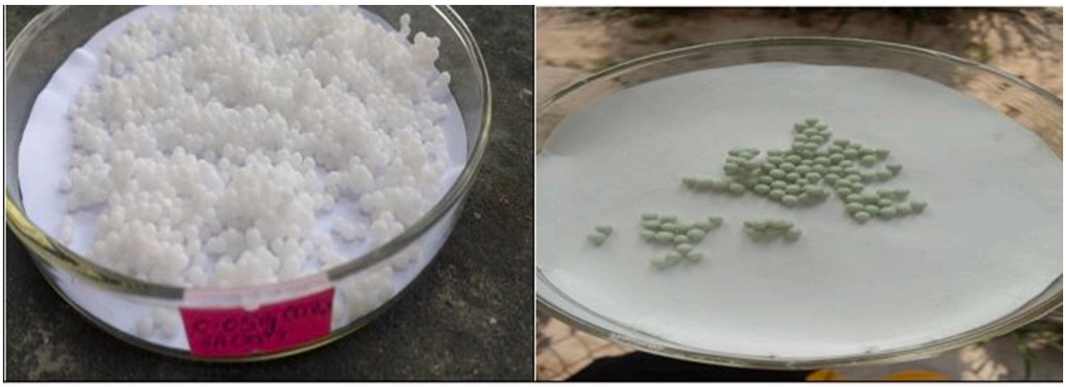

Fig. 2. High resolution optical images of 3NMC-MCA-TiO_2 hydrogel composite beads: (a) before Cu(II) sorption, (b) After Cu(II) sorption.

shaking 180 mg freshly prepared hydrogel beads with 25 mL of each modelled aqueous Cu(II) solution (25, 50 and 100 mg/L) at room temperature. Several aliquot portions (every time 1.0 mL) of reaction mixture were gathered after specific time periods followed by appropriate dilution and equilibrium concentrations were determined by ICP-OES. Volume correction factor was also taken into account to find out q_t values. The sorption experiments designed for isothermal, kinetic and other sorption studies were carried out in order to investigate suitable conditions for better sorption of metal ions inside the 3D biopolymer matrix. Furthermore, calculations of different sorption experiments were made on dry weight basis of hybrid biosorbent to calculate various sorption parameters as reported previously in literature [34]. Several experiments were conducted in duplicate followed by nonlinear regression analysis engaging Origin software 2017. Errors were estimated through statistical analysis and have been inserted on data points in the form of error bars.

3. Results and discussion

3.1. Material characterization

3.1.1. FT-IR analysis

Fig. 1 shows the FTIR spectra of sorbent (3NMC-MCA-TiO_2) before and after loading of Cu(II) ions. The analysis of characteristic stretching frequencies of different vibrational modes in 3NMC-MCA-TiO_2 and Cu (II) loaded biosorbent was performed in the range of 4000–500 cm^{-1}. In 3NMC-MCA-TiO_2 spectrum, an intense and broad peak at 3500–3150 cm^{-1} is observed by overlapped peaks due to polar -OH, -NH and -NH_2 groups. The peak broadness could be attributed to high density intermolecular hydrogen bonding in modified chitosan and alginate structures. The peak located around 1500–1400 cm^{-1} is the characteristic peak due to stretching frequency of C═S group [25]. Successful adherence of amino-thiocarbamate (-OCS-$NHNH_2$) groups over biosorbent is confirmed by the peaks of C═S, -NH and -NH_2 groups. The other well-known absorption bands at around 1600–1550 cm^{-1} and 1100–1000 cm^{-1} are associated with stretching vibrations of peptide bonds (-CONH) and ethereal linkages (C-O-C), respectively [35]. Absorption bands around 2850–2800 cm^{-1} and 2950–2900 cm^{-1} in the form of two small peaks emerged due to stretching frequency of C—H bonds in methylene (-CH_2) and methine (-CH) groups. Stretching bands in fingerprint region appears at about 590–560 cm^{-1} relates to the intrinsic stretching vibrations of Ti-O-O bonds thus verify the successful intercalation of TiO_2 species over NMC-MCA and existence of strong interactions between TiO_2 based polar groups and binding sites of modified alginate and chitosan [36]. However, it is noteworthy to witness the shifts of many bands in the FTIR spectra after the sorption of Cu (II). The chemical shifts to high wavenumbers and diminished intensities of absorption bands might be attributed to the change in chemical environment of biosorbent. The electron-rich donor sites of biopolymer are prompt to transfer their electron density to vacant orbitals of Cu(II) ions to generate sorbent-Cu bonds by adsorption, complexation or ion-exchange interactions.

3.2. SEM analysis

Optical images of employed freshly prepare hydrogel beads of 3NMC-MCA-TiO_2 before and after copper sorption using high resolution camera are displayed in Fig. 2a-b. The hydrogel beads pose white texture which confirm the successful immobilization of TiO_2 nanoparticles into porous alginate and chitosan network. The hybrid biocomposite beads exhibit uniform and homogeneous texture which might be attributed to the better miscibility and equal distribution of rutile nanoparticles. It might also be the result of strong interactions between hydrophilic TiO_2 species and polar functionalities of NMC-MCA, as reported earlier [36].

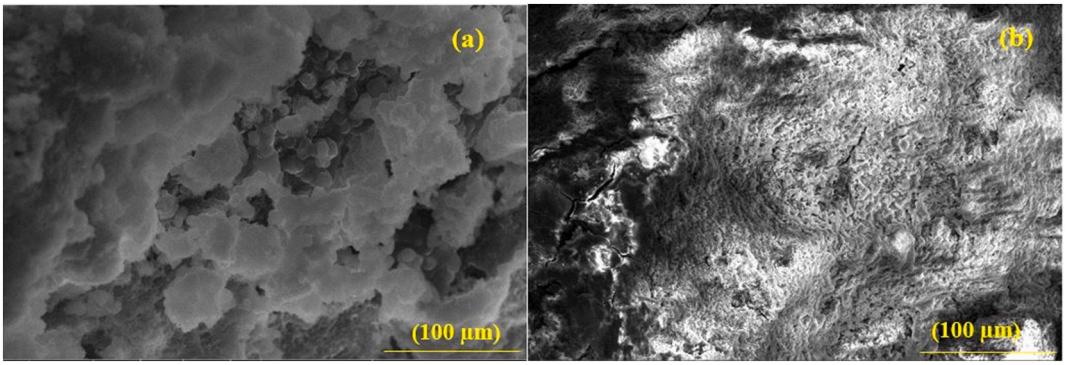

Fig. 3. Magnified SEM images of 3NMC-MCA-TiO_2 hydrogel composite beads: (a) before Cu(II) sorption exposed at the scale of 100 μm, (b) after Cu(II) sorption exposed at the scale of 100 μm.

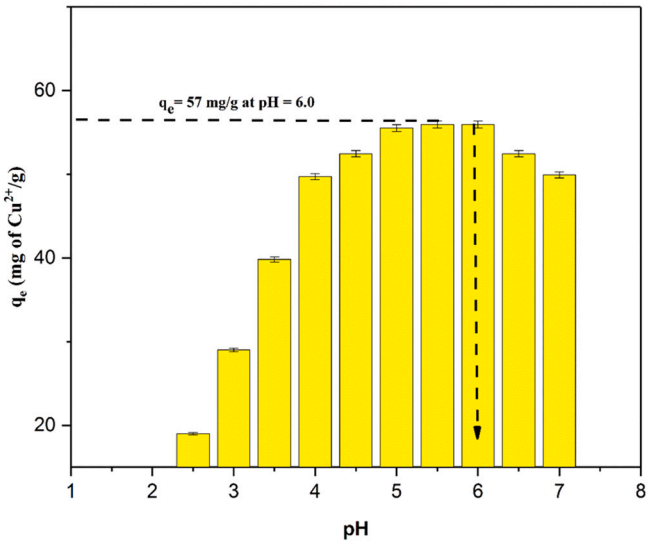

Fig. 4. The effect of equilibrium pH on the sorption capacity (q_e) of 3NMC-MCA-TiO_2 hydrogel composite beads for Cu(II) ions from aqueous solution. (conditions: equilibrium sorption time = 3 h, pH = 2.5–7.0; S.D. = 0.40 g/L; C_o = 100 mg/L; stirring rate = 150 rpm; Temperature = 298 K).

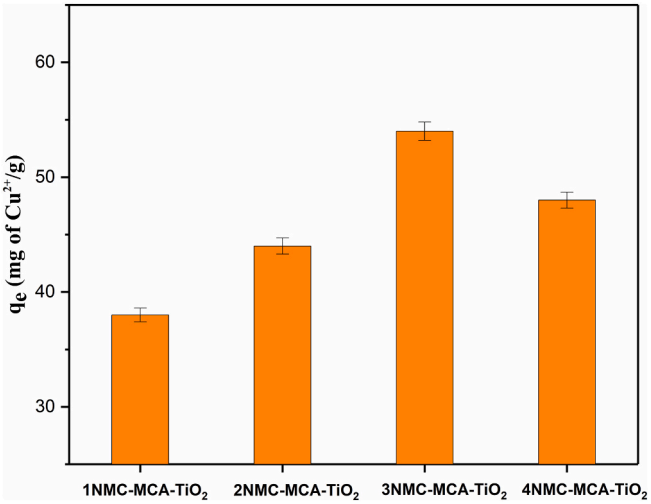

Fig. 5. Effect of TiO_2 to NMC-MCA mass ratio on the sorption capacity during removal of Cu(II) ions from aqueous solution.

The colour transformation of hydrogel beads from white to golden green followed by sorption of Cu(II) is apparent in Fig. 2b. The successful loading of copper species by transfer of electron density from polar functional sites of modified biosorbent holding electron pairs for complexation i.e., −OH, $-NH_2$, $-C=S$, $-OCSNHNH_2$ to electron-deficient central copper metal. Fig. 3a-b show the SEM micrographs of 3NMC-MCA-TiO_2 hydrogel beads before and after the sorption of Cu(II) exposed at the scale of ×10,000 depicting the surface morphological features. By examining the morphology of sorbent in Fig. 3a, surface seems to be quite irregular, convex and widely porous along with intercalated aggregates of rutile nanoparticles into the matrix, indicating strong interactions among polar hydroxyl, amino-thiocarbamate groups and TiO_2 in TSC modified alginate. Heterogeneous distribution of rutile nanoparticles into the three-dimensional network of modified alginate increases the overall surface area and intrinsic diffusional porosity of sorbent that eventually provides more sorption space for copper ions to get adsorbed. Fig. 3b shows an SEM image after sorption where Cu(II) ions filled up the interstitial spaces by forming thin layers and the surface appears relatively uniform, granular and homogeneous. Moreover, slightly swollen porous structures with cracks on sorbent surface followed by sorption could also be observed.

examined by conducting a set of sorption experiments with varying pH from 2.5 to 7.0 at room temperature. The range of this working pH was selected to avoid Cu(II) precipitation to its hydroxide $Cu(OH)_2$ at pH above 7.0. The trend of changes in sorption capacity (q_e) of produced hybrid biosorbent for Cu(II) ions sorption with equilibrium pH is shown in Fig. 4. The graph reveals that sorption capacity (q_e) for hybrid biosorbent is greatly influenced by solution pH owing to metal ion chemistry in solution. The sorption capacity increases gradually with increase in pH till the maximum value of sorption capacity q_m (57 mg/g) was observed at pH 5.5–6.0. At pH ≤ 2.5 small yet appreciable sorption capacity (10–12 g/mg) is observed, this is because some Cu(II) species might produce anionic complexes $[CuCl_3]^-$ with free Cl^- in solution and then get exchanged with counter anion (Cl^-) of protonated functional groups. Moreover, sorption capacity was obvious low because of repulsive forces among Cu^{2+} species and positive charge bearing sorbent surface at low pH. This can be explained on account of proton uptake by primary binding sites of hybrid biosorbent (-OH, $-NH_2$, -COOH, C═S, -O-CS-$NHNH_2$) in the presence of high concentration of powerful reducing H^+ ion activity and subsequent change into protonated forms i.e., $-OH_2^+$, $-NH_3^+$, $-COOH_2^+$, $C{=}SH^+$, $-OCSNHNH_3^+$. The aforementioned explanation could be proposed in general chemical equations presented as Eqs. (1) to (4):

$$\text{Polymer}-NH_3^+\,Cl^- + [CuCl_3]^- \longrightarrow \text{Polymer}-NH_3^+\,[CuCl_3]^- + Cl^- \quad (1)$$

$$\text{Polymer}-O-CS-NHNH_3^+\,Cl^- + [CuCl_3]^- \longrightarrow \text{Polymer}-O-CS-NHNH_3^+\,[CuCl_3]^- + Cl^- \quad (2)$$

$$\text{Polymer}-O-CS-NHNH_3^+ + Cu^{2+} \longrightarrow 2\,\text{Polymer}-O-CS-NHNH_2.Cu^{2+} + 2H^+ \quad (3)$$

$$\text{Polymer}-COOH + Cu^{2+} \longrightarrow (\text{Polymer}-COO)_2.Cu^{2+} + 2H^+ \quad (4)$$

3.3. Effect of medium pH and Cu(II) uptake mechanism

Medium pH measures the hydrogen ion (H^+) potential in sorption system and pose significant influence on solubility, chemistry, distribution of metal species in solution along with surface charge and binding ability of biosorbent [37]. Therefore, the influence of pH on sorption capacity of 3NMC-MCA-TiO_2 during Cu(II) removal was

However, a gradual increase in sorption capacity of biosorbent from 28 to 57 mg/g was found in the pH range 3.0–6.0. This can be explained by respective decrease in active hydrogen H^+ potential and increased feasibility for Cu^{2+} ions to get chelated with electron rich functional sites over neutral surfaces of modified biosorbent. Therefore, the

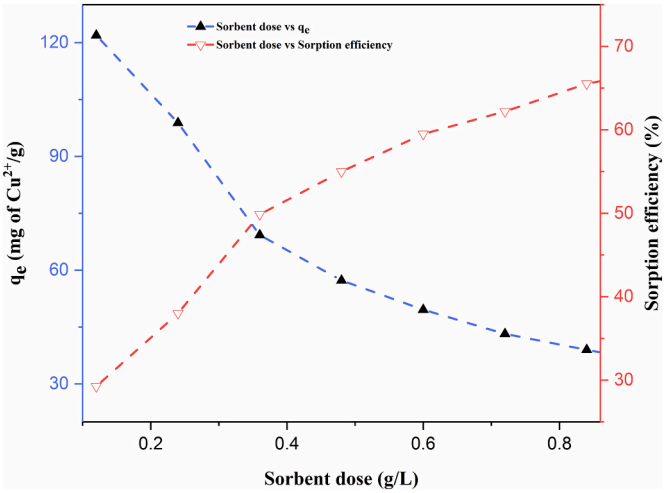

Fig. 6. Effect of 3NMC-MCA-TiO_2 dose on the sorption capacity and sorption efficiency during removal of Cu(II) ions from aqueous solution. (Conditions: pH = 6.0; S.D. = 0.1–0.9 g/L; C_o = 100 mg/L; stirring rate = 150 rpm; Temperature = 298 K).

binding ability of developed sorbent increases with pH up to 6.0 and beyond this value starts dropping due to the formation of insoluble metal hydroxide species i.e., $Cu(OH)_2$. Hence pH 6.0 was found as an optimum value in designing the sorption experiments and elaboration of kinetic, equilibrium and thermodynamic parameters.

3.4. Optimization of TiO_2/NMC-MCA mass ratio and sorbent dose

The variable amounts of rutile (TiO_2) i.e., 0.050, 0.075, 0.100, 0.150 g were immobilized in constant mass of modified hybrid composite (NMC-MCA) to get different composition of NMC-MCA-TiO_2. (5.0–15.0 % by weight). The role of composition upon sorption capacity is shown in Fig. 5, it is obvious from the plot that sorption capacity increases with the increase in TiO_2 amount till the prominent increased sorption capacity was obtained using 3NMC-MCA-TiO_2 hydrogel beads for Cu(II) sorption (i.e.,10.0 % by weight of modified biopolymer). Heavy metal removal from wastewater is much dependent on sorbent dosage (S.D.) of sorbent especially at commercial scale [38]. Hence, optimization of sorbent dose was a key contributing factor for acquiring prominent removal efficiency and sorption capacity of Cu(II) using 3NMC-MCA-TiO_2 hydrogel beads. Multiple adsorption-desorption, ion exchange and other mechanisms are involved in the sorption process before the equilibrium stage [39]. At environmental scale, sorbent with appreciable S.D. values ensure a high sorption efficiency while dealing with extremely low metal ion concentrations sorbents with high sorption capacities are preferred. Therefore, the relationship among sorption capacity and sorption efficiency versus sorbent dose was studied. The sorption capacity decreases with increase in sorbent amount for given volume of solution using 3NMC-MCA-TiO_2 hydrogel beads in the range 0.1–0.85 g/L as shown in Fig. 6. Maximum sorption capacity of 120 mg/g was observed when 0.1 g/L sorbent was employed and it further dropped to 34 mg/g at S.D. value of 0.85 g/L. This downfall of q_e might speculate that plenty of Cu(II) species are present over the sorbent surface forming aggregates so not enough free metal ions are available to saturate the active sites of composite biosorbent. The active functional sites like amino-thiocarbamate (-O-CS-$NHNH_2$) grafted over sorbent might not find sufficient Cu^{2+} ions to interact with and form complexes. The negligible q_e values after a certain value of S.D. suggests that C_e is no more dependent on sorbent concentration. Moreover, sorption efficiency increases gradually with increase in sorbent dose but this trend gradually slows down, as shown in Fig. 6. Increase in sorbent dose of 3NMC-MCA-TiO_2 hydrogel beads from 0.1 to 0.85 g/L increases the sorption efficiency for Cu(II) from 30 % to 66 %. This ascending curve for removal efficiency might be indication of abundant and readily available sorbent binding sites for Cu(II). Finally, 0.35 g/L sorbent dose of 3NMC-MCA-TiO_2 was found effective to achieve high values of both sorption efficiency and sorption capacity for Cu(II), and were preferred for further kinetic and equilibrium studies.

3.5. Kinetic study

Sorption kinetics helps to evaluate the rate of sorption, time required to attain the equilibrium stage and intrinsic sorption mechanisms under different metal concentrations in aqueous solution [40]. Each sorption experiment with different set of Cu(II) concentration was carried out in

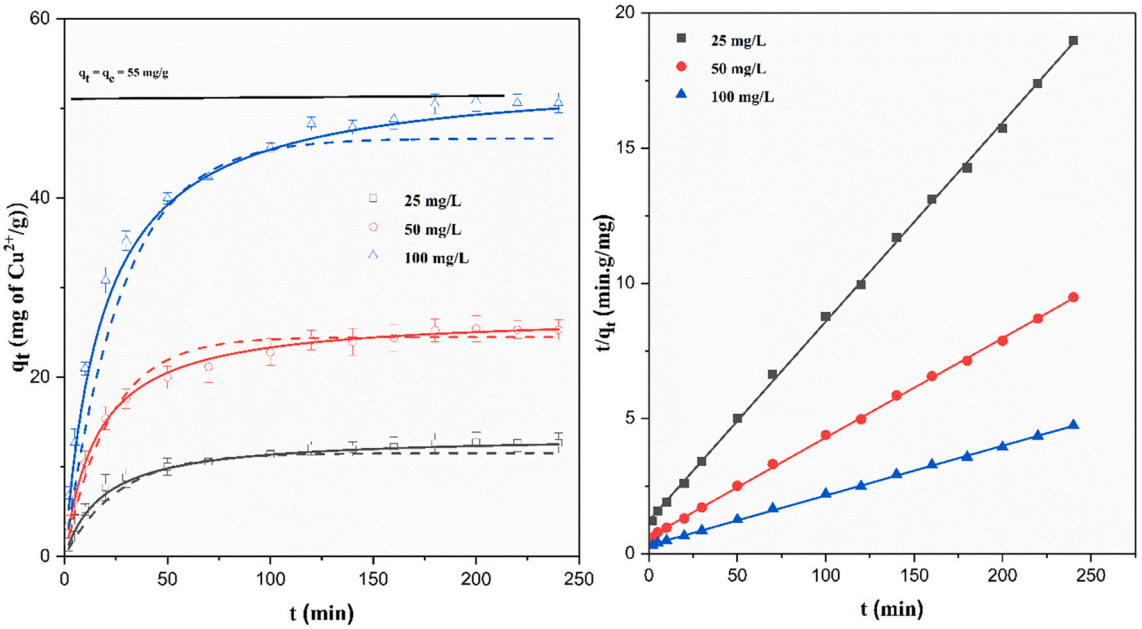

Fig. 7. The nonlinear and linear kinetic profiles of Cu(II) sorption using 3NMC-MCA-TiO_2 hydrogel composite beads for different initial metal concentrations i.e., 25, 50 and 100 mg/L, where PSORE and PFORE models are simulated by solid and dotted lines, respectively.

Table 1
Kinetic models parameters for Cu(II) sorption using 3NMC-MCA-TiO_2.

Sorbent					
	PFORE				
	C_o (mg/L)	$q_{e1\ exp}$ (mg/g)	$k_1 \times 10^{-2}$ (min^{-1})	$q_{e\ cal}$ (mg/g)	R^2
	25	12	4.602 ± 0.007	11.52 ± 0.32	0.91
	50	25	5.429 ± 0.004	24.48 ± 0.40	0.97
	100	53	4.318 ± 0.006	46.64 ± 1.33	0.91
	PSORE				
	C_o (mg/L)	$q_{e2\ exp}$ (mg/g)	$k_2 \times 10^{-3}$(g/mg. min^{-1})	$q_{e\ cal}$ (mg/g)	R^2
	25	12	3.97 ± 0.003	13.47 ± 0.21	0.99
	50	25	2.32 ± 0.009	27.03 ± 0.17	0.99
	100	53	0.99 ± 0.009	53.88 ± 0.85	0.99
	RID (W & M plot)				
	C_o (mg/L)		k_{id} (mg/g· $min^{-0.5}$)	C	R^2
3NMC-MCA-TiO_2			2.00 ± 0.05	−1.15 ± 0.17	0.99
	25		3.97 ± 0.08	−2.28 ± 0.27	0.99
			8.01 ± 0.22	−4.62 ± 0.65	0.99
			0.58 ± 0.06	5.70 ± 0.54	0.97
	50		1.29 ± 0.16	10.61 ± 1.12	0.96
			2.22 ± 0.31	23.75 ± 2.62	0.96
			0.25 ± 0.03	9.03 ± 0.45	0.86
	100		0.39 ± 0.07	19.47 ± 0.97	0.80
			1.00 ± 0.14	36.12 ± 1.80	0.86
	Elovich model				
	C_o (mg/L)	β (g/mg)	α (mg/ g min^{-1})		R^2
	25	0.40	2.50		0.98
	50	0.21	1.08		0.98
	100	0.10	10.44		0.98

duplicate. The kinetic sorption profiles reveal change in instantaneous sorption capacity (q_t) of 3NMC-MCA-TiO_2 with respect to contact time (t) at various initial Cu(II) concentrations i.e., 25, 50 and 100 mg/L as shown in Fig. 7. The rising kinetic profiles could be segmented into three separate small segments of time for better explanation of sorption regimes. Rapid sorption was observed during initial 15 min, gradual increase in sorption capacity that is from 1 to 5, 1–10 and 1–20 mg/g is observed at initial Cu(II) concentration of 25, 50 and 100 mg/L, respectively. It might be due to the availability of unoccupied active sites or absence of any intrinsic diffusion resistance for accessibility of metal ions to sorbent surface. However, as sorption proceeds the binding sites gradually get occupied and subsequent deceleration in sorption rates is observed. Therefore, in next 15–30 min sorption continues at relatively slower rates and sorption capacity increases from 5 to 8, 10–18 and 20–35 mg/g for 25, 50 and 100 mg/L of Cu(II) initial concentration, respectively. A further decrease in sorption rate was experienced from 30 min to onward contact time and sluggish increase in q_t was recorded until it reached the equilibrium stage in 3 h. When all the active sites are engaged with metal ions, surface of hydrogel beads becomes saturated and kinetic curve could be perceived parallel to time axis. The sorption capacity values of 3NMC-MCA-TiO_2 hydrogel beads at equilibrium were found to be 12, 25 and 53 mg/g at 25, 50 and 100 mg/L of Cu(II) ion concentration. Agitation of adsorption system was set at appropriate

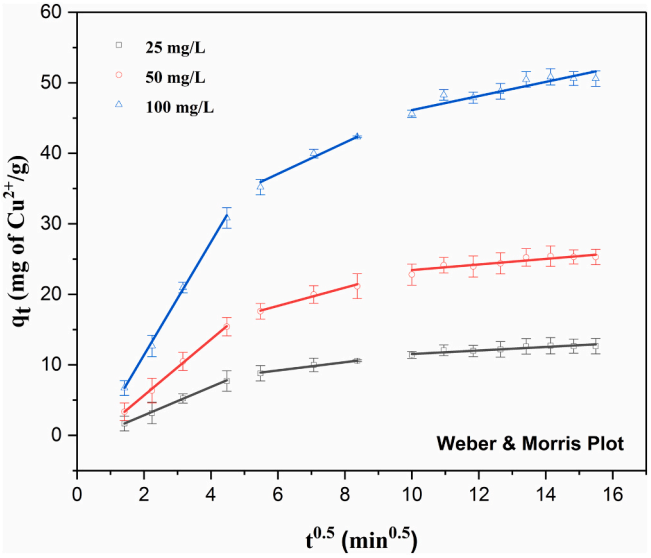

Fig. 8. Weber and Morris plots for depicting the role of intra-particle diffusion for Cu(II) sorption using 3NMC-MCA-TiO_2 hydrogel composite beads for different initial metal concentrations i.e., C_o = 25, 50 and 100 mg/L.

rate, so possibility of bulk/film diffusion by metal aggregation or precipitation could be simply neglected. Aiming to discover the main contributing factors upon sorption mechanism before equilibrium, conventional kinetic sorption models i.e., pseudo first order (PFO), pseudo second order (PSO), resistance to intra-particle diffusion equation (RIDE) and Elovich chemisorption models were engaged to interpret the sorption data.

Lagergren PFORE and Blanchard PSORE, rate equations are presented as Eqs. (5) & (6) respectively [41].

$$\frac{dq_t}{dt} = k_1\,(q_e - q_t) \tag{5}$$

$$\frac{dq_t}{dt} = k_2\,(q_e - q_t)^2 \tag{6}$$

After integration and by applying boundary conditions on Eqs. (5) & (6), linear expressions for PFORE and PSORE can be written as Eqs. (7) and (8), respectively.

$$log(q_e - q_t) = log(q_e) - \left(\frac{k_1}{2.303}\right)t \tag{7}$$

$$\frac{t}{q_t} = \frac{1}{k_2 q_e^2} + \frac{t}{q_e} \tag{8}$$

where, q_t and q_e represent the amounts of Cu(II) adsorbed per unit weight of 3NMC-MCA-TiO_2 at any instant t and at equilibrium, while k_1 and k_2 are the rate constants for PFORE and PSORE expressions, respectively.

The kinetic profiles of Cu(II) sorption using 3NMC-MCA-TiO_2 hydrogel composite beads for different initial metal concentrations i.e., 25, 50, 100 mg/L, where PSORE and PFORE models are simulated by solid and dotted lines, respectively, are shown in Fig. 7, while the evaluated kinetic parameters using different kinetic models are summarized in Table 1. It could be established that R^2 for PSORE is relatively higher and closer to one than that obtained by applying PFORE. Moreover, estimated q_e values by engagement of PSO rate equation seems more comparable with experimentally measured q_e values. It indicates that PSORE model shows better agreement with kinetic phenomenon and rate limiting step depends on intrinsic chemisorption instead of simple bulk/film diffusion as per PSO assumptions. Various chelating sites over 3NMC-MCA-TiO_2 like amino, hydroxyl, amino-thiocarbamate

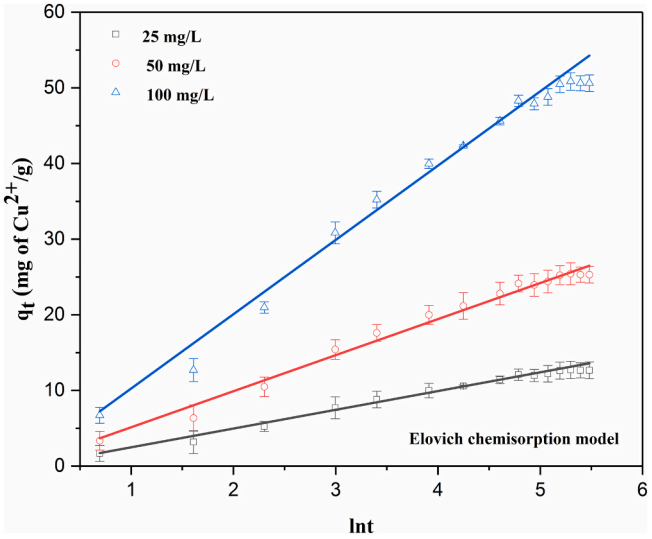

Fig. 9. Linear Elovich chemisorption plots for Cu(II) sorption using 3NMC-MCA-TiO_2 hydrogel composite beads using different initial metal concentrations i.e., C_o = 25, 50 and 100 mg/L.

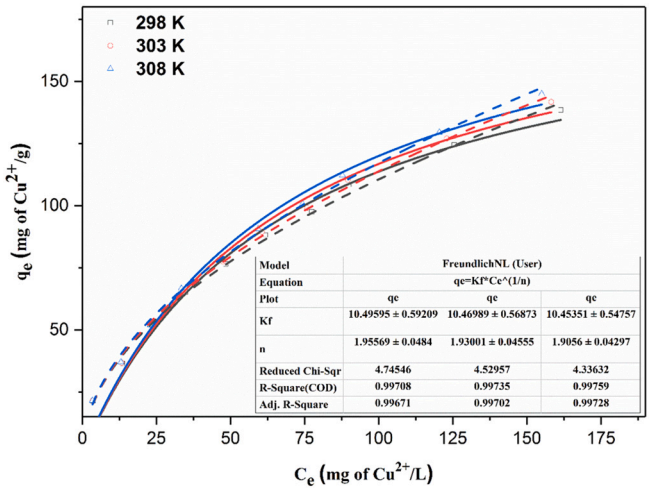

Fig. 10. Equilibrium Cu(II) sorption profiles using 3NMC-MCA-TiO_2 (Conditions: pH = 6.0; S.D. = 0.40 g/L; C_o = 100 mg/L; stirring = 150 rpm; Temp. = 298, 303 and 308 K). Langmuir and Freundlich models are simulated by solid and dotted lines, respectively.

etc., are involved in sorption of Cu(II) by complex formation, however, oxidation state of Cu, density and nature of sorbent chelating sites have significant impact on sorption rates. Decrease in k_2 values i.e., 3.97 $\pm 0.003\times10^{-3}$, $2.32\pm0.009\times10^{-3}$ and $0.99\pm0.009\times10^{-3}$ g/mg.min^{-1} at 25, 50 and 100 g/L of Cu(II), respectively, show that sorption rates for Cu(II) decrease with increase in initial concentration.

Contribution from Intra-particle diffusion in sorption rate was analysed by applying kinetic data to RIDE model. Fickian's RIDE equation is presented as Eq. (9) [42].

$$q_t = k_{id} t^{0.5} + C \tag{9}$$

where, q_t is the adsorbed amount of Cu(II) per unit weight of biosorbent at time t (mg/g), k_{id} is the RIDE constant and C is the intercept of plot q_t vs $t^{0.5}$. Fig. 8 shows Webber and Morris plot of q_t vs $t^{0.5}$ sectioned into multi-linear segments with each affording different values of slopes and intercepts which indirectly supports the presence of variable pore sizes and diverse porous regimes over the surface of hybrid biosorbent.

Table 2
The sorption parameters obtained by applying data to Freundlich and Langmuir models during Cu(II) sorption using 3NMC-MCA-TiO_2 at different temperatures.

Sorbent					
3NMC-MCA-TiO_2	Langmuir				
	Temp. (K)	q_m (mg/g)	$K_L \times 10^{-2}$ (L/mg)		R^2
	298	191.50 ± 12.60	1.46 ± 0.0002		0.98
	303	198.15 ± 13.28	1.43 ± 0.0002		0.98
	308	204.94 ± 13.98	1.41 ± 0.0002		0.98
		Freundlich			
	Temp. (K)	K_f (mg^{1-n} L^n /g)	n	1/n	R^2
	298	10.49 ± 0.59	1.95 ± 0.04	0.51	0.99
	303	10.46 ± 0.56	1.93 ± 0.04	0.52	0.99
	308	10.45 ± 0.54	1.90 ± 0.04	0.53	0.99

Table 1 presents the values of R^2 for RID profile along with K_{id} and C. Data indicates that resistance to pore diffusion is prominent in the start when fast kinetics is observed due to the porous sites for metal attachment and three-dimensional porous structure of biosorbent. However, with adsorption of Cu(II) role of diffusion resistance become insignificant and sorption rates are decelerated. Moreover, the first linear segments in RID kinetic profile do not pass through the origin and might suggest that sorption rates cannot be explained solely by RID model.

Further kinetic studies data was applied to Elovich Chemisorption model presented as Eq. (10) [43].

$$qt = \frac{1}{\beta} ln(\alpha\beta) + \frac{1}{\beta} ln(t) \tag{10}$$

where, α and β are initial adsorption rate constant and desorption constant, respectively. The Elovich kinetic profiles for Cu(II) sorption over composite beads are shown in Fig. 9. The evaluated values of initial adsorption rate constant (α) and Elovich constant (β) for different Cu(II) concentration are given in Table. 1. It is evident that ascending values for α (2.50, 1.08, 10.44 mg/g.min^{-1}) are relatively higher than β (0.40, 0.21, 0.10 g/mg), respectively. It might be deduced that 3NMC-MCA-TiO_2 exhibits plenty of functional sites over the surface like amino -NH_2, hydroxyl -OH, carboxyl -COOH, amino-thiocarbamate -O-CS-$NHNH_2$ etc., which are easily accessible to Cu(II) ions for developing interactions and get chemically adsorbed.

3.6. Adsorption study

Sorption isotherms provide an insight into extent of metal ions adsorption onto biosorbent surface and affinity of metal ions with sorbent active sites at different operational temperatures revealing valuable information about sorption process. Isothermal sorption profiles in the form of nonlinear plots between equilibrium sorption capacity (q_e) of 3NMC-MCA-TiO_2 hydrogel beads and equilibrium concentration (C_e) at different temperatures i.e., 298, 303 and 308 K are shown in Fig. 10. The progressive increase in q_e with C_e corresponds to Type-I type sorption isotherm. The profiles tend to be flatten upon achieving sorption desorption equilibria. The sorption data was interpreted using different sorption models such as Langmuir, Freundlich, Redlich-Peterson, Dubinin-Radushkevich and Temkin model. The sorption data could be well explained using Langmuir and Freundlich models, nonlinear expressions of these two models are expressed in Eqs. (11) and (12), respectively.

$$q_e = \frac{q_m k_L C_e}{1 + k_L C_e} \tag{11}$$

$$q_e = k_f C_e^{\frac{1}{n}} \tag{12}$$

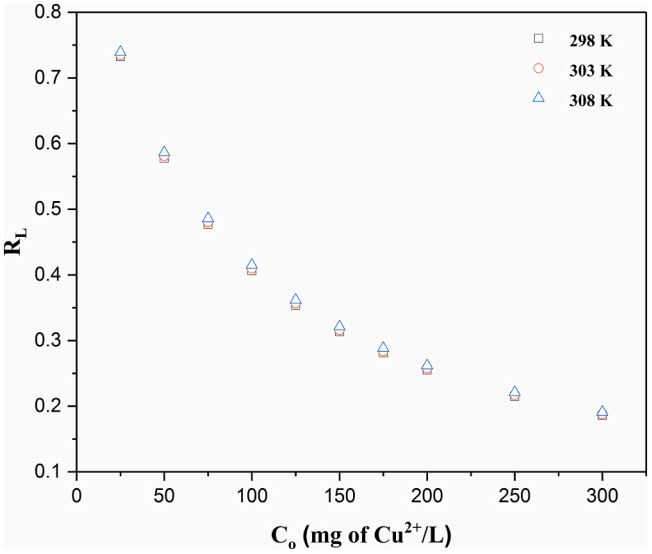

Fig. 11. Plot showing the variation of Langmuir equilibrium constant (R_L) against initial Cu(II) concentration (C_o, mg/L).

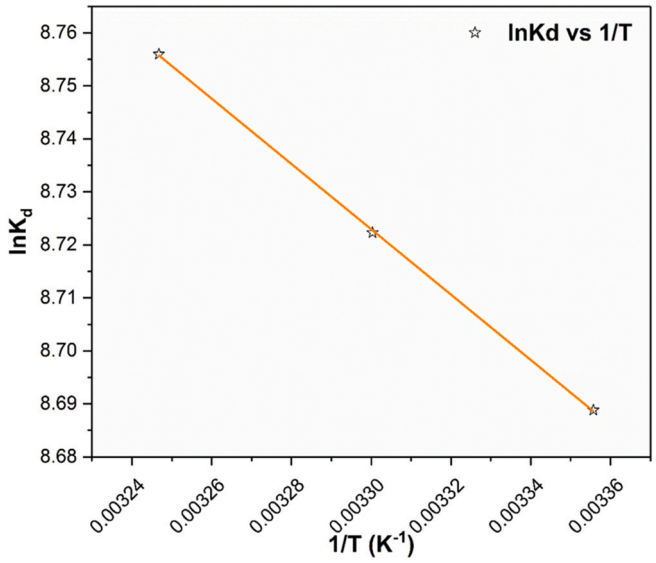

Fig. 12. The plot lnK_d vs. 1/T (K^{-1}) for Cu(II) sorption from aqueous solution using 3NMC-MCA-TiO_2.

In these mathematical expressions q_e represents the adsorbed amount of Cu(II) in mg/g using 3NMC-MCA-TiO_2 at sorption desorption equilibrium, q_m is the maximum amount of Cu(II) in mg/g which occurs because of monolayer sorption on 3NMC-MCA-TiO_2. Langmuir constant k_L (L/mg) depict the extent of binding strength during metal sorbent adsorbate interface. K_f ($mg^{1-n}.L^n/g$) is known as Freundlich empirical constant which measures the relative affinity of metal ions to sorbent surfaces and 1/n is the heterogeneity factor. Langmuir dimensionless separation factor (R_L) measures the suitability of selected sorbent towards target metal ions. It reveals that whether sorption is irreversible ($R_L = 0$), favourable ($0 < R_L < 1$) or linear ($R_L = 1$). Meanwhile, heterogeneity factor ($0 < 1/n < 1$) also measures the tendency of sorption system to be favourable. The obtained equilibrium sorption parameters i.e., q_m, K_L, K_f and n are given in Table. 2. These parameters were evaluated through nonlinear fitting of the experimental data, where solid and dotted lines correspond to the curves by applying Langmuir and Freundlich expressions, respectively. The fitness of the curve could be judged using correlation coefficient (R^2). It is evident from the Table 2 that sorption data of Cu(II) using 3NMC-MCA-TiO_2 is in close agreement with Freundlich model ($R^2 \approx 0.99$) as compared to Langmuir model. It proposes that principal sorption phenomenon at heterogeneous surface of newly developed 3NMC-MCA-TiO_2 hydrogel beads comprised of strong chemical interactions and chemisorption is the main mode of sorption. Moreover, mutual interactions between adsorbate species and non-identical sorbent binding sites also exist. Empirical values of 1/n factor were found between 0 and 1 which suggest the favourable copper sorption. The obtained K_f values i.e., 10.49 ± 0.59, 10.46 ± 0.56 and 10.45 ± 0.54 $mg^{1-n}.L^n/g$ at 298, 303 and 308 K, respectively, suggest the existence of strong attractive forces between Cu (II) ions and sorbent active sites. Moreover, experimental Cu(II) sorption findings also fall in good agreement with Langmuir model ($R^2 \approx 0.98$). So, it may be speculated that 3NMC-MCA-TiO_2 composite hydrogel beads might exhibit a definite number of active sites with identical energies with each site being occupied by single solute specie without any lateral interaction among solute molecules. Moreover, sorption is supposed to be monolayer, sorption mechanism is expected to be pure chemisorption and sorption system approaches state of dynamic equilibrium as sorption and desorption of ions is reversible. Fig. 11 signifies a non-linear plot of dimensionless parameter R_L against a range of initial Cu(II) concentrations (C_o) at different temperatures, which shows the favourable sorption of Cu(II) over 3NMC-MCA-TiO_2 beads at all temperatures. The maximum monolayer sorption capacity (q_m) values for

Table 3
Thermodynamic parameters ΔH^o, ΔG^o, and ΔS^o for Cu(II) sorption using 3NMC-MCA-TiO_2.

Temp. (K)	ΔG^o (kJ/mol)	ΔH^o (kJ/mol)	ΔS^o (kJ/mol. K)	$T\Delta S^o$ (kJ/mol)	R^2
298	−21.53	5.12	0.09	26.82	0.99
303	−21.97			27.27	
308	−22.42			27.72	

Cu(II) at different temperatures (298, 303 and 308 K) were computed as 192, 198 and 205 mg/g. It shows the substantial binding strength of functional sites for Cu(II) ions exist at all temperatures. Moreover, 3NMC-MCA-TiO_2 beads exhibit promising sorption capacity for Cu^{2+} in comparison to pure alginate ($q_m = 106$ mg/g) [40], and other previously reported modified alginate based biosorbents for instance SA-PAM/GO hydrogel composites ($q_m = 68.76$ mg/g) [44], amine-based functionalized graphene oxide/alginate hybrid composite GO-HMDA ($q_m = 98.18$ mg/g) [45], core/shell-like alginate@polyethylenimine composites ($q_m = 163.7$ mg/g) [46] and functionalized Polyvinyl alcohol/sodium alginate beads ($q_m = 97.2$ mg/g) [47]. Table 4 summarizes the comparative performance of 3NMC-MCA-TiO_2 with other sorbents of similar structure.

Since, the feasibility of sorption is associated with Gibbs free energy change (ΔG^o) whereas standard enthalpy (ΔH^o) and standard entropy change (ΔS^o) provide an insight into heat changes involved during sorption process and randomness at sorbent adsorbate interface, respectively. Thermodynamic parameters were evaluated using Van't Hoff equation and Gibbs free energy equation, expressed as Eqs. (14) and (15):

$$lnK_d = -\frac{\Delta H^\circ}{RT} + \frac{\Delta S^\circ}{R} \tag{14}$$

$$\Delta G^\circ = \Delta H^\circ - T\Delta S^\circ \tag{15}$$

where T is temperature in Kelvin scale, K_d is the distribution constant and R is known as general gas constant (8.314 J/mol.K). Fig. 12 reveals a linear trend between lnK_d vs. 1/T. ΔH^o and ΔS^o values were computed from slope and intercept of plot lnK_d vs. 1/T. while ΔG^o was calculated by utilizing the expression of Gibbs free energy change. The respective increase in ΔG^o values (−21.53, −21.97, −22.42 kJ/mol) at different

Table 4
Comparison of 3NMC-MCA-TiO_2 with recently reported alginate-based sorbents for sorption of Cu(II) from aqueous solutions.

Sr. No.	Sorbent	Sorption model	Kinetic model	t_{eq} (min)	pH	q_m[mg Cu(II)/g]	Ref.
1.	Magnetic silica coated iron carbide/alginate beads	Sips	PSO	60	4.5	37.73	[48]
2.	Sodium alginate/poly vinyl alcohol//$KMnO_4$ biochar	Langmuir	PSO	1440	6.0	87.07	[49]
3.	Poly-vinyl alcohol/alginate/poly-acrylamide	Freundlich	PSO	720	5.0	79.5	[50]
4.	Alginate/starch ether composite (HIPS/SA) hydrogel beads	Langmuir	PSO	720	5.5	25.81	[51]
5.	Alginate-g-poly(N-isopropylacrylamide) graft copolymer	Langmuir	–	–	4.5	50.0	[52]
6.	Mag-Ben/CCS/Alg hydrogel beads	Langmuir	PSO	90	5.0	56.79	[53]
7.	Alginate/graphitic carbon nitride composites	Langmuir	PSO	110	6.0	168.2	[54]
8.	Polyethyleneimine modified cellulose/sodium alginate (PEI-RCSA) hydrogel	Langmuir	PSO	480	5.5	177.1	[55]
9.	GO@PAN-PPy/SA nanocomposite hydrogels	Freundlich	PSO	360	3.0	87.2	[56]
10.	3NMC-MCA-TiO_2	Freundlich	PSO	180	6.0	192	This study

temperatures suggests that sorption of Cu(II) is spontaneous and feasible. Besides, positive ΔH^o (+5.12 kJ/mol) and ΔS^o (+0.09 kJ/mol. K) correspond to an endothermic system with increase in randomness at the metal-sorbent interface (Table 3).

4. Conclusion

A hybrid biocomposite based on N-maleated chitosan, amino-thiocarbamate functionalised calcium alginate and anhydrous titania nanoparticles was fabricated. Organo-functionalisation of base biopolymers was carried out using maleic anhydride and Thiosemicarbazide, respectively. Modified sorbent provided excellent support for titania immobilization. Kinetic data illustrated the manifestation of intrinsic chemisorption instead of simple bulk/film diffusion. Equilibrium sorption data fitted well with Freundlich adsorption model ($R^2 \approx 0.99$) which designates the heterogeneous nature of sorbent. Maximum sorption capacity of biosorbent was found 192 mg/g at 298 K and pH = 6.0 Standard Gibbs free energy change ΔG^o(−21.53, −21.97, and − 22.42 kJ/mol), standard enthalpy change ΔH^o(5.12 kJ/mol) and standard entropy change ΔS^o(0.09 kJ/mol K^{-1}) values suggested that the adsorption process was spontaneous and endothermic. The sorbent 3NMC-MCA-TiO_2 could be competitive candidate for economical and rapid adsorptive removal of Cu(II) from dilute effluents.

CRediT authorship contribution statement

Hamza Shehzad: Conceptualization, Data curation, Investigation. **Zahoor H. Farooqi:** Funding acquisition, Writing-review & editing. **Ejaz Ahmed:** Project administration. **Ahsan Sharif:** Supervision. **Muhammad Ajmal:** *V*alidation, Software. **Sana Razzaq:** Formal analysis. **M. Uzair Naseer:** Methodology. **M. Ahmad Nazir:** Formal analysis. **Mehwish Batool:** Methodology. **Tehreem Akram:** Data curation. **Qamar un Nissa:** Investigation. **Amarah Fatima:** Methodology. **Laiba Akbar:** Visualization.

Acknowledgment

Authors are thankful to University of the Punjab, Lahore (No.D/72/Est. I dated 14-01-2022) and Higher Education Commission, Pakistan (No. 20-3995/NRPU/R&D/HEC/14/1212) for funding to carry out this work.

References

[1] A. Verma, S. Thakur, G. Mamba, Prateek, R.K. Gupta, P. Thakur, V.K. Thakur, Graphite modified sodium alginate hydrogel composite for efficient removal of malachite green dye, Int. J. Biol. Macromol. 148 (2020) 1130–1139.
[2] S. Aggarwal, A. Chakravarty, S. Ikram, A comprehensive review on incredible renewable carriers as promising platforms for enzyme immobilization & thereof strategies, Int. J. Biol. Macromol. 167 (2021) 962–986.
[3] S. Sharma, A. Bhattacharya, Drinking water contamination and treatment techniques, Appl. Water Sci. 7 (2017) 1043–1067.
[4] K. Dermentzis, Removal of nickel from electroplating rinse waters using electrostatic shielding electrodialysis/electrodeionization, J. Hazard. Mater. 173 (2010) 647–652.
[5] H. Wu, W. Wang, Y. Huang, G. Han, S. Yang, S. Su, H. Sana, W. Peng, Y. Cao, J. Liu, Comprehensive evaluation on a prospective precipitation-flotation process for metal-ions removal from wastewater simulants, J. Hazard. Mater. 371 (2019) 592–602.
[6] S. Ladislas, C. Gérente, F. Chazarenc, J. Brisson, Y. Andrès, Floating treatment wetlands for heavy metal removal in highway stormwater ponds, Ecol. Eng. 80 (2015) 85–91.
[7] L. Charerntanyarak, Heavy metals removal by chemical coagulation and precipitation, Water Sci. Technol. 39 (1999) 135–138.
[8] D. Ning, C. Yang, H. Wu, Ultrafast Cu^{2+} recovery from waste water by jet electrodeposition, Sep. Purif. Technol. 220 (2019) 217–221.
[9] A.M. Elgarahy, K.Z. Elwakeel, S.H. Mohammad, G.A. Elshoubaky, A critical review of biosorption of dyes, heavy metals and metalloids from wastewater as an efficient and green process, Clean. Eng. Technol. 4 (2021), 100209.
[10] M. Mohsen-Nia, P. Montazeri, H. Modarress, Removal of Cu^{2+} and Ni^{2+} from wastewater with a chelating agent and reverse osmosis processes, Desalination 217 (2007) 276–281.
[11] A.E. Burakov, E.V. Galunin, I.V. Burakova, A.E. Kucherova, S. Agarwal, A. G. Tkachev, V.K. Gupta, Adsorption of heavy metals on conventional and nanostructured materials for wastewater treatment purposes: a review, Ecotoxicol. Environ. Saf. 148 (2018) 702–712.
[12] N. Ates, N. Uzal, Removal of heavy metals from aluminum anodic oxidation wastewaters by membrane filtration, Environ. Sci. Pollut. Res. 25 (2018) 22259–22272.
[13] C. Duan, T. Ma, J. Wang, Y. Zhou, Removal of heavy metals from aqueous solution using carbon-based adsorbents: a review, J. Water Process Eng. 37 (2020), 101339.
[14] B.O. Otunola, O.O. Ololade, A review on the application of clay minerals as heavy metal adsorbents for remediation purposes, Environ. Technol. Innov. 18 (2020), 100692.
[15] Ł. Trybułowski, W. Rogowska, J. Zakrzewski, Biosorption capacity of activated sludge sand bed for removal of copper from treated wastewater, J. Ecol. Eng. 23 (2022) 61–69.
[16] S. Guo, Z. Dan, N. Duan, G. Chen, W. Gao, W. Zhao, Zn(II), Pb(II), and Cd(II) adsorption from aqueous solution by magnetic silica gel: preparation, characterization, and adsorption, Environ. Sci. Pollut. Res. 25 (2018) 30938–30948.
[17] Y. Kobayashi, F. Ogata, T. Nakamura, N. Kawasaki, Synthesis of novel zeolites produced from fly ash by hydrothermal treatment in alkaline solution and its evaluation as an adsorbent for heavy metal removal, J. Environ. Chem. Eng. 8 (2020), 103687.
[18] F.I.A.M.Aisha MuthanaAlasadi1, Adsorption of Cu(II), Ni(II) and Zn(II) ions by nano kaolinite: thermodynamics and kinetics studies, Chem. Int. 5 (2019) 258–268.
[19] B. Qiu, X. Tao, H. Wang, W. Li, X. Ding, H. Chu, Biochar as a low-cost adsorbent for aqueous heavy metal removal: a review, J. Anal. Appl. Pyrolysis 155 (2021), 105081.
[20] R. Wang, R. Liang, T. Dai, J. Chen, X. Shuai, C. Liu, Pectin-based adsorbents for heavy metal ions: a review, Trends Food Sci. Technol. 91 (2019) 319–329.
[21] B.M.W.P.K. Amarasinghe, R.A. Williams, Tea waste as a low cost adsorbent for the removal of Cu and Pb from wastewater, Chem. Eng. J. 132 (2007) 299–309.
[22] E. Ragheb, M. Shamsipur, F. Jalali, F. Mousavi, Modified magnetic-metal organic framework as a green and efficient adsorbent for removal of heavy metals, J. Environ. Chem. Eng. 10 (2022), 107297.
[23] S. Thakur, B. Sharma, A. Verma, J. Chaudhary, S. Tamulevicius, V.K. Thakur, Recent progress in sodium alginate based sustainable hydrogels for environmental applications, J. Clean. Prod. 198 (2018) 143–159.
[24] I.O. Saheed, W. Da Oh, F.B.M. Suah, Chitosan modifications for adsorption of pollutants – a review, J. Hazard. Mater. 408 (2021), 124889.
[25] B.M. Córdova, C.R. Jacinto, H. Alarcón, I.M. Mejía, R.C. López, D. de Oliveira Silva, E. Cavalheiro, T. Venâncio, J.Z. Dávalos, A.C. Valderrama, Chemical modification of sodium alginate with thiosemicarbazide for the removal of Pb(II) and Cd(II) from aqueous solutions, Int. J. Biol. Macromol. 120 (2018) 2259–2270.

[26] X. Gao, C. Guo, J. Hao, Z. Zhao, H. Long, M. Li, Adsorption of heavy metal ions by sodium alginate based adsorbent-a review and new perspectives, Int. J. Biol. Macromol. 164 (2020) 4423–4434.
[27] B. Wang, Y. Wan, Y. Zheng, X. Lee, T. Liu, Z. Yu, J. Huang, Y.S. Ok, J. Chen, B. Gao, Alginate-based composites for environmental applications: a critical review, Crit. Rev. Environ. Sci. Technol. 49 (2019) 318–356.
[28] Y. Zhao, L. Zhan, Z. Xue, K.K. Yusef, H. Hu, M. Wu, Adsorption of Cu (II) and Cd (II) from wastewater by sodium alginate modified materials, J. Chem. 2020 (2020), 5496712.
[29] Y. Li, F. Liu, B. Xia, Q. Du, P. Zhang, D. Wang, Z. Wang, Y. Xia, Removal of copper from aqueous solution by carbon nanotube/calcium alginate composites, J. Hazard. Mater. 177 (2010) 876–880.
[30] H. Basu, R.K. Singhal, M.V. Pimple, S. Saha, Graphene oxide encapsulated in alginate beads for enhanced sorption of uranium from different aquatic environments, J. Environ. Chem. Eng. 6 (2018) 1625–1633.
[31] M. Kragović, S. Pašalić, M. Marković, M. Petrović, B. Nedeljković, M. Momčilović, M. Stojmenović, Natural and modified zeolite—alginate composites. Application for removal of heavy metal cations from contaminated water solutions, Minerals 8 (2018) 1–16.
[32] H. Shehzad, L. Zhou, Z. Li, Q. Chen, Y. Wang, Z. Liu, A.A. Adesina, Effective adsorption of U(VI) from aqueous solution using magnetic chitosan nanoparticles grafted with maleic anhydride: equilibrium, kinetic and thermodynamic studies, J. Radioanal. Nucl. Chem. 315 (2018) 195–206.
[33] H. Shehzad, E. Ahmed, A. Sharif, Z.H. Farooqi, M. Imran, R. Begum, Z. Liu, L. Zhou, J. Ouyang, A. Irfan, I. Nawaz, Modified alginate-chitosan-TiO_2 composites for adsorptive removal of Ni (II) ions from aqueous medium, Int. J. Biol. Macromol. 194 (2022) 117–127.
[34] Y. Luo, H. Li, M. Wu, W. Wang, L. Wang, Selective adsorption and separation of Cr (VI) by surface-imprinted microsphere based on thiosemicarbazide-functionalized sodium alginate, Environ. Technol. 43 (2022) 1140–1151.
[35] H. Shehzad, L. Zhou, Y. Wang, J. Ouyang, G. Huang, Z. Liu, Z. Li, Effective biosorption of U(VI) from aqueous solution using calcium alginate hydrogel beads grafted with amino-carbamate moieties, J. Radioanal. Nucl. Chem. 321 (2019) 605–615.
[36] H. Shehzad, Z.H. Farooqi, E. Ahmed, A. Sharif, M.I. Din, M. Arshad, J. Nisar, L. Zhou, W. Yun, I. Nawaz, M. Hadayat, K. Shahid, Fabrication of a novel hybrid biocomposite based on amino-thiocarbamate derivative of alginate/carboxymethyl chitosan/TiO_2 for Ni(II) recovery, Int. J. Biol. Macromol. 152 (2020) 380–392.
[37] T. Alp Arıcı, A.S. Özcan, A. Özcan, Biosorption characteristics of Cu(II) and Cd(II) ions by modified alginate, J. Polym. Environ. 28 (2020) 3221–3234.
[38] M. Liua, Y. Wena, X. Songa, J.-L. Zhua, J. Li, A smart thermoresponsive adsorption system for efficient copper ion removal based on alginate-g-poly(N-isopropylacrylamide) graft copolymer, Carbohydr. Polym. 219 (2019) 280–289.
[39] B.M. Córdova, T. Venâncio, M. Olivera, R.G. Huamani-Palomino, A.C. Valderrama, Xanthation of alginate for heavy metal ions removal. Characterization of xanthate-modified alginates and its metal derivatives, Int. J. Biol. Macromol. 169 (2021) 130–142.
[40] C.E.R. Barquilha, E.S. Cossich, C.R.G. Tavares, E.A. da Silva, Biosorption of nickel (II) and copper(II) ions from synthetic and real effluents by alginate-based biosorbent produced from seaweed Sargassum sp, Environ. Sci. Pollut. Res. 26 (2019) 11100–11112.
[41] J. Lin, L. Wang, Comparison between linear and non-linear forms of pseudo-first-order and pseudo-second-order adsorption kinetic models for the removal of methylene blue by activated carbon, Front. Environ. Sci. Eng. China 3 (2009) 320–324.
[42] W. Zhu, J. Liu, M. Li, Fundamental studies of novel zwitterionic hybrid membranes: kinetic model and mechanism insights into strontium removal, Sci. World J. 2014 (2014), 485820.
[43] F.C. Wu, R.L. Tseng, R.S. Juang, Characteristics of Elovich equation used for the analysis of adsorption kinetics in dye-chitosan systems, Chem. Eng. J. 150 (2009) 366–373.
[44] H. Jiang, Y. Yang, Z. Lin, B. Zhao, J. Wang, J. Xie, A. Zhang, Preparation of a novel bio-adsorbent of sodium alginate grafted polyacrylamide/graphene oxide hydrogel for the adsorption of heavy metal ion, Sci. Total Environ. 744 (2020), 140653.
[45] M. Majdoub, A. Amedlous, Z. Anfar, A. Jada, N. El Alem, Engineering of amine-based binding chemistry on functionalized graphene oxide/alginate hybrids for simultaneous and efficient removal of trace heavy metals: towards drinking water, J. Colloid Interface Sci. 589 (2021) 511–524.
[46] X. Jiang, Q. Da An, Z.Y. Xiao, S.R. Zhai, Z. Shi, Versatile core/shell-like alginate@polyethylenimine composites for efficient removal of multiple heavy metal ions (Pb^{2+}, Cu^{2+}, CrO_4^{2-}): batch and fixed-bed studies, Mater. Res. Bull. 118 (2019), 110526.
[47] H. Isawi, Using zeolite/polyvinyl alcohol/sodium alginate nanocomposite beads for removal of some heavy metals from wastewater, Arab. J. Chem. 13 (2020) 5691–5716.
[48] F. Ahmadpoor, S.A. Shojaosadati, S.Z. Mousavi, Magnetic silica coated iron carbide/alginate beads: synthesis and application for adsorption of Cu (II) from aqueous solutions, Int. J. Biol. Macromol. 128 (2019) 941–947.
[49] Z. Xiao, L. Zhang, L. Wu, D. Chen, Adsorptive removal of Cu(II) from aqueous solutions using a novel macroporous bead adsorbent based on poly(vinyl alcohol)/sodium alginate/$KMnO_4$ modified biochar, J. Taiwan Inst. Chem. Eng. 102 (2019) 110–117.
[50] W. Zhang, Q. Deng, Q. He, J. Song, S. Zhang, H. Wang, J. Zhou, H. Zhang, A facile synthesis of core-shell/bead-like poly (vinyl alcohol)/alginate@PAM with good adsorption capacity, high adaptability and stability towards Cu(II) removal, Chem. Eng. J. 351 (2018) 462–472.
[51] M. Dai, Y. Liu, B. Ju, Y. Tian, Preparation of thermoresponsive alginate/starch ether composite hydrogel and its application to the removal of Cu(II) from aqueous solution, Bioresour. Technol. 294 (2019), 122192.
[52] M. Liu, Y. Wen, X. Song, J. Zhu, J. Li, A smart thermoresponsive adsorption system for efficient copper ion removal based on alginate-g-poly(N-isopropylacrylamide) graft copolymer, Carbohydr. Polym. 219 (2019) 280–289.
[53] H. Zhang, A.M. Omer, Z. Hu, L.Y. Yang, C. Ji, X.kun Ouyang, Fabrication of magnetic bentonite/carboxymethyl chitosan/sodium alginate hydrogel beads for Cu (II)adsorption, Int. J. Biol. Macromol. 135 (2019) 490–500.
[54] W. Shen, Q. Da An, Z.Y. Xiao, S.R. Zhai, J.A. Hao, Y. Tong, Alginate modified graphitic carbon nitride composite hydrogels for efficient removal of Pb(II), Ni(II) and Cu(II) from water, Int. J. Biol. Macromol. 148 (2020) 1298–1306.
[55] W. Zhan, C. Xu, G. Qian, G. Huang, X. Tang, B. Lin, Adsorption of Cu(ii), Zn(ii), and Pb(ii) from aqueous single and binary metal solutions by regenerated cellulose and sodium alginate chemically modified with polyethyleneimine, RSC Adv. 8 (2018) 18723–18733.
[56] W. Zhang, J. Ou, B. Wang, H. Wang, Q. He, J. Song, H. Zhang, M. Tang, L. Zhou, Y. Gao, S. Sun, Efficient heavy metal removal from water by alginate-based porous nanocomposite hydrogels: the enhanced removal mechanism and influencing factor insight, J. Hazard. Mater. 418 (2021).